LANGMUIR

Interface Components: Nanoparticles, Colloids, Emulsions, Surfactants, Proteins, Polymers

Clearly Detectable, Kinetically Restricted Solid-Solid Phase Transition in cis-Ceramide Monolayers

Maria Laura Fanani, Jon V Busto, Jesús Sot, Jose Luis Abad, Gemma Fabrias, Leonor Saiz, Jose M. G. Vilar, Felix M. Goni, Bruno Maggio, and Alicia Alonso

Langmuir, **Just Accepted Manuscript** • DOI: 10.1021/acs.langmuir.8b02198 • Publication Date (Web): 05 Sep 2018

Clearly Detectable, Kinetically Restricted Solid-Solid Phase Transition in *cis*-Ceramide Monolayers

M. Laura Fanani [#,1,2], Jon V. Busto[#,3,4], Jesús Sot [3], José L. Abad[5], Gemma Fabrías[5,6], Leonor Saiz [7,8], Jose M. G. Vilar[3,4,9], Félix M. Goñi[3,4], Bruno Maggio[1,2], and Alicia Alonso *[,3,4].

[1] Universidad Nacional de Córdoba. Facultad de Ciencias Químicas. Departamento de Química Biológica "Ranwel Caputto". Córdoba, Argentina

[2] CONICET. Universidad Nacional de Córdoba. Centro de Investigaciones en Química Biológica de Córdoba (CIQUIBIC), Córdoba, Argentina.

[3]Instituto Biofisika (CSIC, UPV/EHU), B. Sarriena s/n, 48940 Leioa, Spain.

[4]Departamento de Bioquímica, Universidad del País Vasco, B. Sarriena s/n, 48940 Leioa, Spain.

[5] Research Unit on Bioactive Molecules (RUBAM), Dpto de Química Biológica, Instituto de Química Avanzada de Catalunya (IQAC – CSIC), Barcelona, Spain.

[6]Centro de Investigación Biomédica en Red (CIBERehd).

[7]Modeling of Biological Networks and Systems Therapeutics Laboratory, Department of Biomedical Engineering, University of California, 451 East Health Sciences Drive, Davis, CA 95616, USA.

[8]Institute for Medical Engineering & Science, Massachusetts Institute of Technology, Cambridge, MA 02139, USA

[9]IKERBASQUE, Basque Foundation for Science, 48011, Bilbao, Spain

[#]These two authors contributed equally to this work.

*Corresponding author. E-mail: alicia.alonso@ehu.eus

Abstract

Sphingosine [(2S, 3R, 4E)-2-amino-4-octadecene-1,3-diol] is the most common sphingoid base in mammals. Ceramides are N-acyl sphingosines. Numerous small variations on this canonical structure are known, including the 1-deoxy, the 4,5-dihydro, and many others. However, whenever there is a Δ4 double bond, it adopts the *trans* (or E) configuration. We synthesized a ceramide containing 4Z-sphingosine and palmitic acid (*cis*-pCer) and studied its behaviour in the form of monolayers extended on an air-water interface. *Cis*-pCer acted very differently from the *trans* isomer in that, upon lateral compression of the monolayer, a solid-solid transition was clearly observed at a mean molecular area ≤ 44 $Å^2$.$molecule^{-1}$, whose characteristics depended on the rate of compression. The solid-solid transition, as well as states of domain coexistence, could be imaged by atomic force microscopy and by Brewster-angle microscopy. Atomistic molecular dynamics simulations provided results compatible with the experimentally observed differences between the *cis* and *trans* isomers. The data can help in the exploration of other solid-solid transitions in lipids, both *in vitro* and *in vivo*, that have gone up to now undetected due their less obvious change in surface properties along the transition, as compared to *cis*-pCer.

Introduction

Sphingolipids are important modulators of a large variety of cellular functions.[1,2] Among them ceramide (Cer), a pivotal component in sphingolipid biosynthesis and degradation, has received considerable attention and is a key player in various cell signaling processes.[3–5] It has become increasingly clear that many sphingolipid actions are strongly related to their capacity to modulate the physical properties of cell membranes,[6–9] thus the regulation of membrane-associated enzymatic activities mediating the formation of signaling molecules.[1–3,10]

In particular, regulation of the membrane lateral heterogeneity by Cer has gathered attention over the last two decades.[9,11] Cer generation upon sphingomyelinase enzymatic activity has been proposed to induce membrane leakage, transbilayer (flip-flop) lipid motion[6,8] and time-dependent highly-ordered segregated lateral structures[10,12,13] putatively involved in the regulation of enzyme activities and membrane platform formation prior to lipid-mediated cell signalling.[14–16] A complex thermotropic behavior was observed for the fully hydrated *trans*- palmitoyl ceramide (*trans*-pCer). A metastable bilayer gel phase exists at low temperatures, while an exothermic transition occurs at 64°C to form a stable bilayer, probably chain tilted with respect to the bilayer normal. Further increases in temperature lead to a disordered (likely H_{II}-type) chain-melted phase above ≈90°C.[17,18] Despite the molecular shape of pCer, with a small polar head group and a relatively large hydrocarbon moiety, that is unfavorable for forming bilayers, it can be readily spread on the water surface to form Langmuir monolayers. The latter have been proven to be adequate models[19] for studying in-plane phase transitions, surface topography as well as membrane mechanical, electrostatic and viscoelastic properties.[20] Recently, elegant studies of membrane elasticity of Cer films permit to univocally classify Cer monolayers as 2D solids able to undergo plastic deformation, unlike typical fluid lipid monolayers.[21–23]

In our previous study[24] it was mentioned that pure *trans*-pCer monolayers exhibited an isothermal condensed-condensed phase transition at room temperature. Such

transition occurred at ≈40°C below the gel-fluid transition observed for bulk aqueous dispersions of *trans*-pCer.[17] Further studies with different types of *trans*-Cer showed that these compounds can exhibit a rich variety of surface pressure- and temperature-dependent monolayer and bulk phase states and surface electrostatics depending on the acyl chain length and unsaturation.[25–29] In particular, *trans*-pCer undergoes a formerly neglected second (or higher) order liquid-condensed (LC) → solid (S) phase transition at about room temperature while a first order liquid-expanded (LE) → LC transition occurs over a range of temperatures encompassing the physiological one.[26] A solid-solid phase transition accompanied by chain packing alterations from orthorhombic to hexagonal subcells for pure Cer membranes was also reported to occur 20-25 °C below the main order-disorder transition in a detailed study using Fourier transformed infrared spectroscopy.[30] Interestingly, recent studies have proposed that a high proportion of tightly packed orthorhombic phase, brought about by the presence of ~30 mol% of long-chain Cer appears essential for the maintenance of the impermeability properties in model stratum corneum membranes.[31]

The study of solid-solid lipid phase transitions has been scarcely explored for lipid membranes since it usually involves only subtle changes of molecular volume, which results in low entropy changes. The present work originated from our curiosity on the biophysical properties of *cis*-ceramides. Nature offers many variations in ceramide structure, i.e. chain length, presence or absence of the Δ4-double bond, 2 or 3 hydroxy groups, and so on,[32] but, to our knowledge, whenever the Δ4-double bond exists, it is in the *trans* form. This is in contrast with most double bonds found in lipids, which have *a cis* configuration (i. e. fatty acids, plasmenyl-phospholipids, etc.). The basis for the *trans* configuration of the C4 double bond of natural sphingolipids could be unveiled by investigating the biophysical properties of the *cis*-isomers and their biological consequences. The cell signaling properties of Cer are critically affected by the double bond between C4 and C5 of the sphingoid chain. The change of the natural *trans* configuration to *cis* or the saturation of the double bond decreased the affinity of brain ceramidase

toward its substrate.[33] In a previous study[34] we had examined the conformational impact of the *cis* double bond in hydrated ceramides by multidimensional ^{1}H and ^{13}C NMR spectroscopy. Unlike *trans*-Cer, the *cis*-isomer exhibited not one but two broad yet resolved resonances for the protons in C1-OH and C3-OH, much like dihydroceramide. The results indicated that the *cis* double bond twisted, slightly, the orientation of C1-OH with respect to C3-OH, thus weakening the hydrogen-bonding network formed between the two OH groups of *cis*-Cer and bound water molecules. In the current paper we describe the properties of monolayers consisting of *cis*-pCer, the 4,5- *cis* sphingoid base isomer of the more usual *trans*-pCer. We found that *cis*-pCer exhibited a kinetically-restricted solid-solid phase transition with unusually large changes of molecular area under isothermal compression, and marked hysteresis. The present study furthers our understanding of solid-solid lipid phase transitions, and can be of relevance for the interpretation of more nuanced transitions in naturally occurring sphingolipids.

Materials and Methods

Chemicals.

Trans-pCer (N-palmitoyl-D-*erythro*-sphingosine) was provided by Avanti Polar Lipids, Inc (Alabaster, AL, USA) and used without further purification. The water was purified by a Milli-Q (Millipore, Billerica, MA, USA) system, to yield a product with a resistivity of ~18.5 MΩ-cm and a surface tension of 72.8 mN/m at 25°C. Other chemicals were of the highest purity available.

Synthesis of Δ4-cis-pCer.

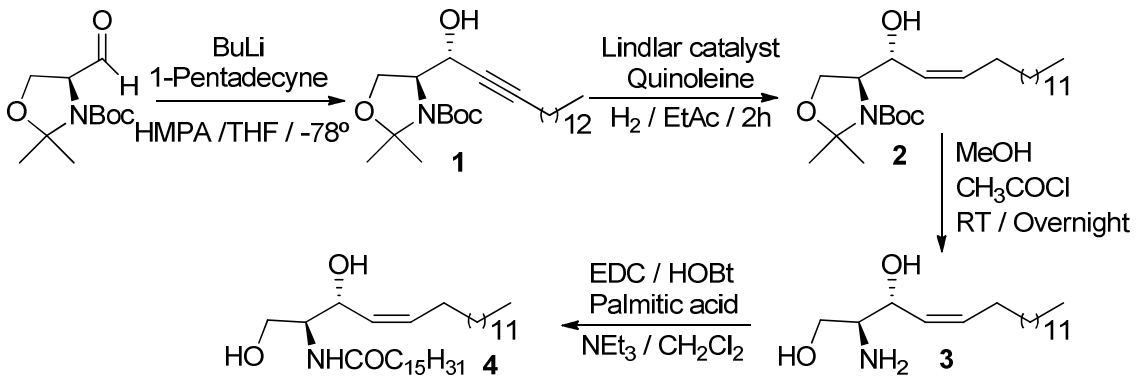

Scheme 1. Synthesis of Δ4-*cis*-pCer.

Preparation of Δ4-*cis*-2*S*,3*R*-C16 ceramide was carried out according to the synthetic pathway depicted in the Scheme 1. Thus, following the procedure described by Herold, 2*S*-Garner Aldehyde was reacted with pentadecyne treated with BuLi in the presence of HMPA to afford compound **1**. Reduction of alkyne **1** with Lindlar catalyst in presence of quinoleine under H_2 atmospheric pressure gave rise to the *cis*-alkene intermediate **2**. Deprotection with CH_3COCl in CH_3OH as a source of HCl provided the *cis*-2*S*,3*R*-sphingosine **3** after basic treatment. Condensation of **3** with palmitic acid was achieved by using the system EDC/HOBt as a coupling agent in presence of NEt_3 to afford the corresponding *cis*-C16-ceramide **4**.

Stereoselective catalytic hydrogenation to the cis double bond

To a solution of the corresponding allylic alcohol (1.3 mmol) in degassed EtAc (50mL) Lindlar catalyst (5 % w/w) and quinoleine were added (1% w/v), purged with two H_2 flask volumes and the mixture stirred for 2 h at room temperature under the same atmosphere (balloon). The reaction mixture was then filtered through Celite® bed and the particles were rinsed with EtAc (3 x 5 mL). The combined filtrates were concentrated *in vacuo* to give a residue, which was purified by flash chromatography on silica gel (from 0 to 30 % EtOAc in hexane), yielding the desired compound.

(S)-tert-butyl 4-((R,E)-1-hydroxyhexadec-2-en-1-yl)-2,2-dimethyloxazolidine-3-carboxylate **2:** ^{1}H NMR (400 MHz, $CDCl_3$) (mixture of rotamers) δ 5.56 (m, 1H), 5.40 (1H, t, *J*= 10 Hz), 4.67 (bs, 1/3H, rotamer), 4.57 (bs, 2/3H, rotamer), 4.12 (bs, 1H), 4.00 (bs, 1H), 3.82 (bs, 1H), 2.11 (m, 2H), 1.55 (br, 3H), 1.49 (bs, 12H), 1.37 (m, 2H), 1.25 (bs, 20H), 0.88 (t, 3H, *J*= 7.0 Hz)

^{13}C NMR (101 MHz, $CDCl_3$) (mixture of rotamers) δ 154.1, 133.9, 129.2, 128.1, 94.4, 68.2, 64.7, 62.4, 32.0, 29.8, 29.8, 29.7, 29.7, 29.7, 29.6, 29.4, 29.4, 28.5, 28.1, 22.8, 14.2.

HRMS calculated for $C_{26}H_{49}NO_4Na$ ($[M + Na]^+$): 462.3559, found: 462.3549.

Acid-mediated removal of isopropyliden and N-Boc protecting groups

To an ice cooled solution of the corresponding protected aminodiol (1 mmol) in MeOH (40 mL) neat acetyl chloride (5 equiv./mol) was added dropwise. After stirring at room temperature overnight, the reaction mixture was concentrated *in vacuo* to give a crude mixture, which was purified by flash chromatography on silica gel (from 0 to 20 % MeOH in CH_2Cl_2), to afford the required amine hydrochloride.

cis-(2*S*,3*R*)-Sphingosine **3:** ^{1}H NMR (400 MHz, $CDCl_3$) δ 5.59 (dt, 1H, J_1= 11.0 Hz, J_2= 7.5 Hz), 5.41 (1H, t, *J*= 10.0 Hz), 4.48 (m, 1H), 3.77 (bs, 4H), 3.70 (bs, 2H), 2.94 (bs, 1H), 2.06 (m, 2H), 1.38 (m, 2H), 1.25 (bs, 22H), 0.87 (t, 3H, *J*= 7.0 Hz)

^{13}C NMR (101 MHz, $CDCl_3$) δ 134.7, 128.5, 69.1, 62.7, 56.9, 32.1, 29.9, 29.8, 29.8, 29.8, 29.8, 29.6, 29.5, 28.1, 22.8, 14.2.

HRMS calculated for $C_{18}H_{38}NO_2$ ($[M + H]^+$): 300.2903, found: 300.2894.

C16-Ceramide 4 preparation

EDC (1.3 mmol) was added portionwise to a mixture of palmitic acid (1 mmol) and HOBt-hydrate (1.1 mmol) in 10 mL CH_2Cl_2 under argon atmosphere. After stirring

for 5 min, this solution became transparent and was added dropwise over a CH_2Cl_2 solution (10 mL) of the sphingoid base (1 mmol) containing 2 mmol of NEt_3 under the same atmosphere. TLC showed the evolution of the reaction and, after 1 h, water (20 mL) was poured into the reaction mixture. The organic phase was separated and washed with brine (2 x 5 mL), then dried over anhydrous MgSO4 to afford a crude mixture that was purified by flash SiO_2 chromatography (100:1) using an eluent gradient of MeOH in CH_2Cl_2 (0.1% each step). Product appeared at 2.6-3% interval of MeOH (yield 72%).

cis-(2*S*,3*R)*-C16-Ceramide **4:** ^{1}H NMR (400 MHz, $CDCl_3$) δ 6.25 (1H, d, *J*= 8 Hz), 5.58 (dt, 1H, J_1= 11.0 Hz, J_2= 7.5 Hz), 5.47 (1H, m), 4.65 (m, 1H), 3.97 (dd, 2H, J_1= 11.0 Hz, J_2= 3.5 Hz), 3.84 (m, 1H), 3.70 (dd, 2H, J_1= 11.0 Hz, J_2= 3.5 Hz), 2.49 (bs, 1H), 2.21 (t, 1H, *J*= 8 Hz), 2.09 (m, 2H), 1.62 (m, 2H), 1.25 (bs, 50H), 0.87 (t, 6H, *J*= 7.0 Hz)

^{13}C NMR (101 MHz, $CDCl_3$) δ 174.2, 134.7, 128.7, 69.7, 62.6, 55.0, 37.0, 32.1, 29.9, 29.8, 29.8, 29.8, 29.8, 29.7, 29.7, 29.5, 29.5, 29.5, 28.0, 25.9, 22.8, 14.2.

HRMS calculated for $C_{34}H_{68}NO_3$ ($[M + H]^+$): 538.5199, found: 538.5189.

Surface Pressure - Area Isotherms.

Lipid monolayers were prepared and characterized in a Langmuir film balance with uniaxial compression as detailed before [26] onto NaCl 145 mM (pH ~6.5) subphase at (23 ± 1) °C. The surface pressure was determined using the Wilhelmy method with a Pt plate according to eq. 1.

$$\pi = \gamma_0 - \gamma \quad \text{(eq. 1)}$$

where γ_0 and γ denote the surface tension before and after lipid spreading at the interface, respectively. After solvent evaporation and relaxation at $\pi \leq 0.5$ mN/m (~ 5 min), the film was compressed uniaxially at a rate typically of 0.5 ± 0.05 Å^2.molec^{-1}.min^{-1} unless otherwise specified, until reaching the collapse pressure by reducing the area between two Delrin^{TM} barriers. Their lateral movement over the trough

surface was controlled and registered by an electronic unit. The mean molecular area (MMA) was taken as the total monolayer area divided by the total number of molecules spread at the interface. The absence of surface-active impurities in the subphase solutions or in the spreading solvents was checked routinely as described elsewhere.[35] In-plane surface elasticity[36] upon compression was assessed by means of the compressibility modulus (Cs^{-1}), directly calculated from the isotherm data as:

$$C_S^{-1} = -MMA\left(\frac{\delta\pi}{\delta MMA}\right)_T \qquad \text{(eq. 2)}$$

Thermodynamics of Langmuir monolayers.

The free energy of compression (ΔG_{comp}) was calculated as:[37]

$$\Delta G_{comp} = -\int_{A_0}^{A_i} \pi \delta A \qquad \text{(eq. 3)}$$

The area (A) can be taken as the MMA and thus ΔG_{comp} can be calculated as the area under the compression curve between certain limits. In this work, we have taken A_0 and A_i as the MMA at 1 and 30 mN/m, respectively. These limits avoid the rather large errors arising from the gaseous portion of the compression isotherms and incipient instabilities occurring when the film approaches collapse.

In general, for ideally fluid films, the energy given to the system during the compression process (ΔG_{comp}) is equal to the energy returned by the system in the expansion process (ΔG_{expan}). When these quantities are not equal (and $\Delta G_{comp} > \Delta G_{expan}$), a certain amount of energy is stored by the system that is not restored after expansion. This represents the free energy of hysteresis assigned to the compression-expansion cycle and is calculated as follows:[38]

$$\Delta G^{hys} = \Delta G_{expan} - \Delta G_{comp} \qquad \text{(eq. 4)}$$

Brewster angle microscopy (BAM) of lipid films at the air/saline solution interface.

Langmuir monolayers were prepared as described above in a Langmuir equipment mounted on the stage of a Nanofilm EP3 Imaging Ellipsometer

(Accurion, Goettingen, Germany), which was used in the Brewster Angle Microscopy (BAM) mode. Minimum reflection was set with a polarized laser beam (λ = 532 nm) incident on the bare aqueous surface at the experimentally calibrated Brewster angle (~53.1º). The lipid monolayers were spread onto the aqueous surface and compressed to the desired pressure. After monolayer formation and during compression, the reflected light was collected through a 20x objective and an analyser-polariser (A-polariser) lens to a CCD camera. The gray level at each pixel of the BAM images can be converted to reflectivity values with calibration factors tested for each individual experiment.

For 2D isotropic monolayers the reflectivity obtained from BAM measures is related to both the film thickness and to the refractive index (the so called "optical thickness") of the film.[39,40] In films showing 2D anisotropy, where the surface organization is such that the molecular symmetry axis does not coincide with the radiation incidence plane, the reflected light may show a change in the polarization plane due mainly to the refractive index having a different value in the direction of the hydrocarbon chains and in the orthogonal direction. Therefore, in some experiments we set the A-polariser at -45º or +45º from the plane of the incident beam to study the birefringence effects. Image processing and gray level measurements were performed using the free software ImageJ 1.43u (NIH, USA).

Langmuir film transfer to solid supports for Atomic Force Microscopy (AFM) inspection.

Trans- and c*is*-pCer monolayers were prepared by spreading chloroform/methanol (2:1, v/v) solutions of the lipids (1 mg/mL) onto a water subphase in the surface balance (Nima Technology, Coventry, UK). After 10 min to allow for solvent evaporation, monolayers were compressed to the required pressures at a compression rate of 0.5 $Å^2 \cdot molecule^{-1} \cdot min^{-1}$ under equilibrium conditions (allowing film relaxation for 30 min after each $5 mN.m^{-1}$ increase). After 30 min equilibration, the monolayers were transferred to mica V1 quality supports (Electron Microscopy Sciences, Hatfield, USA) that had been previously immersed in the subphase, to

form Langmuir-Blodgett (LB) films, at a transfer speed of 5 mm/min. Unless otherwise stated, the experiments were performed at 22 ± 1°C.

AFM imaging.

The measurements were performed on a NanoWizard II AFM (JPK Instruments, Berlin, Germany) at a controlled temperature of 22 ºC. MLCT silicon nitride cantilevers (Veeco Instruments Inc., Plainview, NY, USA) with spring constants of 0.1 or 0.5 N/m were used in contact mode scanning (constant vertical deflection) to measure the SPBs, continuously maintaining the minimum possible force. 512 x 512 pixel resolution images were collected at a scanning rate between 1 and 1.5 Hz and line-fitted using the JPK Image Processing software as required.

Computational study of pCer monolayers: System set-up and Molecular Dynamics simulation details.

To gain insights into the potential structure, interactions, and organization of the lipids in the monolayer we performed atomistic Molecular Dynamics simulations. We used GROMACS 5.1.1 at a temperature of 295.15 K with GROMOS96 53A6 force field, extended to include Berger lipid parameters. Since the system is expected to be out of equilibrium for the experimental compression/expansion rates, we could not use a traditional equilibration run. Instead, we choose an ordered initial configuration with favorable lipid-lipid interactions. Specifically, we chose an hexagonal packing of the tails with the lipids oriented so that intermolecular amide groups (N-H...O=C; amine and carbonyl groups) could interact. To accommodate this type of packing, we selected an area of 386.621×446.432 $Å^2$ with an array of 72×48 lipids. We removed 4 lipids along the middle axis of the simulation box to introduce defects that could facilitate the formation of disordered domains. This resulted in a simulation box with a total of 3,452 lipids with an area per lipid of 50 $Å^2$. As initial structure of the lipid molecule, we removed the extra atoms of lignoceroyl fatty acid chain of a configuration of the

ceramide NS (24:0) lipid (N-lignoceroyl-D-*erythro*-sphingosine) of Faller and coworkers,[41] which was used for both palmitoylated *cis* (*cis*-pCer) and *trans* (*trans*-pCer) isomers of Cer (C16 ceramide, N-palmitoyl-D-*erythro*-sphingosine). The resulting monolayer was then hydrated with a 40-Å thick simple point charge (SPC) water slab. Differences between *cis* and *trans* forms of pCer were introduced at the level of ITP files, which were obtained by modifying accordingly the ITP files of Faller and coworkers.[41] We performed energy minimization followed by a total simulation time of 2 ns with a 2 fs time step in the NVT ensemble for both *cis*-pCer and *trans*-pCer monolayers.

Results and Discussion

Isothermal compression of cis-pCer monolayers.

When *cis*-pCer is spread at the air/ saline solution interface a stable monomolecular film is formed. The film exhibits negligible desorption into the subphase after compression/expansion cycles (not shown). When compressed from an excess area condition (≥ 50 $Å^2$.molecule^{-1}) at a relatively high compression rate the isotherms show a characteristic two-dimensional diffuse phase transition, that occurs over a rather narrow range of mean molecular areas (MMA). Figure 1 shows the compression curves of *cis*-pCer at different compression rates, together with that of *trans*-pCer for comparison. At the working temperature the latter shows a solid character and a very subtle second (or higher) order LC - S phase transition at ~ 15 mN/m[26] over a similar range of MMA.

Unexpectedly, at compression rates ≤ 4 $Å^2$.molecule^{-1}.min^{-1} a valley (decrease of surface pressure under reduction of MMA) is observed in the compression isotherm of *cis*-pCer over the phase coexistence region (Figure 1a). This probably arises from an out-of-equilibrium condition of the molecular organization adopted under the compression process, pointing to a kinetically restricted formation of the phase state formed at MMA ≤ 44 $Å^2$.molecule^{-1}. Furthermore, the characteristics of the closely packed phase state appear to depend on its rate of formation. Under a

relatively fast compression rate, the resulting state shows lower compressibility modulus values (Cs^{-1}), than those formed at slower compression rates (Figure 1b). This reflects the adoption of a different inner structure by the kinetically-limited state.

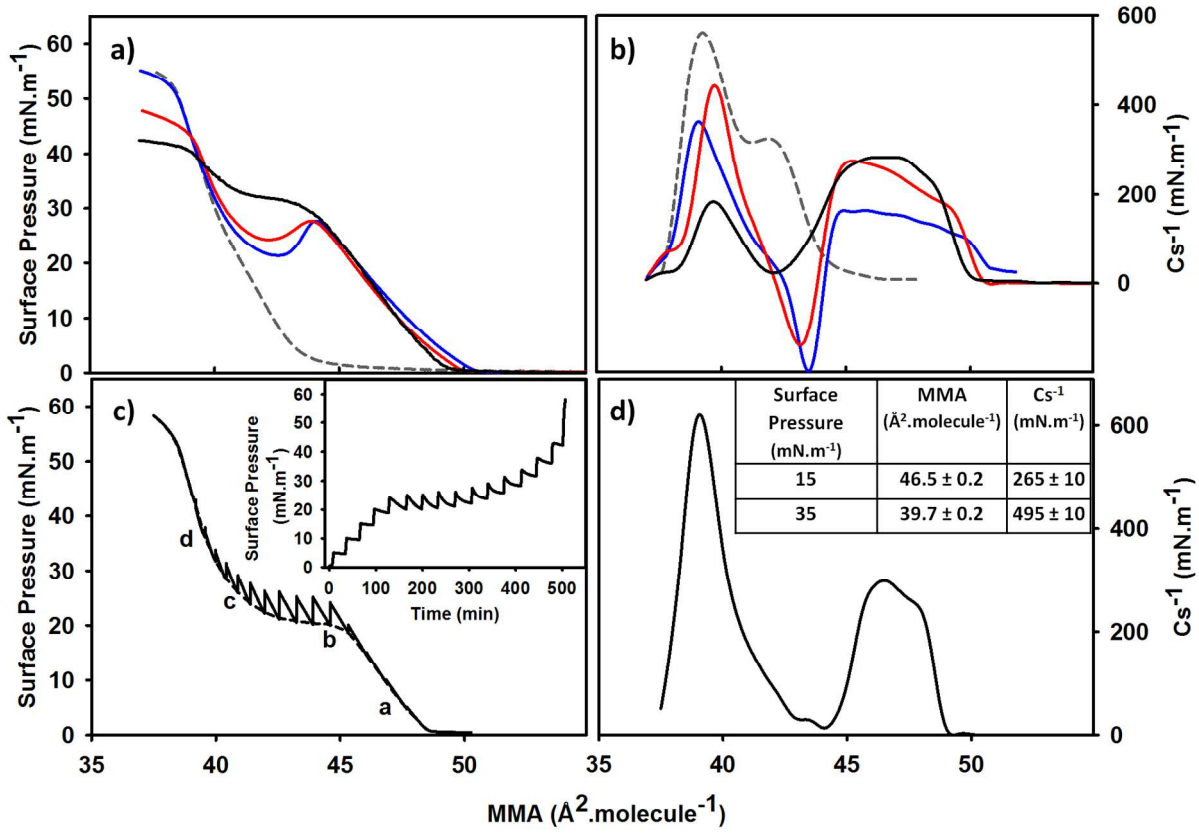

Figure 1. Dependence of *cis*-pCer surface behaviour on the compression rate. Compression isotherms (a) and compressibility modulus calculated after eq. 2 (b) of *cis*-pCer Langmuir monolayers at compression rates of 13 (black), 2.5 (red) or 0.5 (blue lines) $Å^2.molecule^{-1}.min^{-1}$. The dashed gray lines correspond to *trans*-pCer Langmuir film (data taken from Ref.[26]). c) Compression isotherm of *cis*-pCer monolayer after stepwise relaxation (30 min relaxation after each ~5 mN/m surface pressure increase) at a compression rate of 0.5 $Å^2.molecule^{-1}.min^{-1}$(solid black line). The inset shows the time curve of the process. The black dashed line shows the extrapolated isotherm constructed by taking into account only the points after relaxation (equilibrium isotherm). Letters mark the stages imaged by BAM as shown in Figure 3. d) Compressibility modulus (Cs^{-1}) calculated from the equilibrium isotherm in c). Statistics of the MMA and Cs^{-1} data of the phases formed at low and high surface pressure at equilibrium are shown in the inset in (d). Working temperature: 22 ± 1 C°. The plot shows representative experiments that do not differ in more than 0.2 $Å^2.molecule^{-1}$ from their replicas.

In order to get an insight into the thermodynamic and rheological properties of the phase transition undergone by *cis*-pCer monolayers, we performed a compression-interrupted experiment allowing relaxation of the film for 30 min after short periods of slow compression (see Figure 1c). By taking into account only the data after annealing we constructed a compression isotherm for *cis*-pCer monolayers under equilibrium conditions.

The elastic response upon a dilatation stress of the film under equilibrium conditions, measured by the compressibility modulus, provides information on the phase state of the film. For LC and S monolayers a large increase of surface pressure is induced by a small reduction of the monolayer area.[36] Figure 1d shows that at a low surface pressure and ~46 $Å^2$.molecule^{-1}, the film shows characteristics of a LC or soft S phase with Cs^{-1} ~ 260 mN/m (from now phase S1), while at high surface pressure and ~ 40 $Å^2$.molecule^{-1}, which is close to the lower limit for the cross sectional area of a two-chained lipid, a more typical solid phase with Cs^{-1} ~ 500 mN/m is observed (from now phase S2). The latter phase closely resembles the one formed by *trans*-Cer,[25,26] as is also apparent from a closer analysis of Figure 1b.

In a previous work, a detailed analysis of the isotherm and isobar curves of *trans*-pCer suggested the presence of a second (or higher) order LC $\rightarrow$ S phase transition at room temperature,[24] which showed a rise in the Cs^{-1} of the film from ~ 400 to ~ 600 mN/m over scarcely 3 $Å^2$.molecule^{-1} during compression (from 43 to 40 $Å^2$.molecule^{-1}).[26] Only 65 ± 8 cal.mol^{-1} was necessary to compress a *trans*-pCer from 1 to 35 mN/m. This is the Gibbs free energy of compression (ΔG_{comp}) and according to Gaines[36] it operationally represents the two-dimensional work involved in bringing together the film-forming molecules from a loosely packed state to the closer molecular packing at the higher pressure. This thermodynamic quantity is a complex parameter reflecting the energy balance between intermolecular interactions, the loss of entropy upon compression and the energy related to phase transitions.

Under equilibrium conditions (as shown in figure 1c), a larger amount of energy is necessary to compress a *cis*-pCer monolayer (ΔG_{comp} = 115 ± 5 cal.mol^{-1}), but the amount is small when compared to the one required to compress *trans*-oleoyl Cer from an LE to an LC phase (ΔG_{comp} = 300 ± 5 cal.mol^{-1}) which involves a reduction of molecular area from ~ 48 to 40 Å^2.molecule^{-1}.[27] Those different ΔG_{comp} may be directly related to the change in molecular volume experienced by the Cer molecules during the phase transition, thus to the entropy loss upon compression.

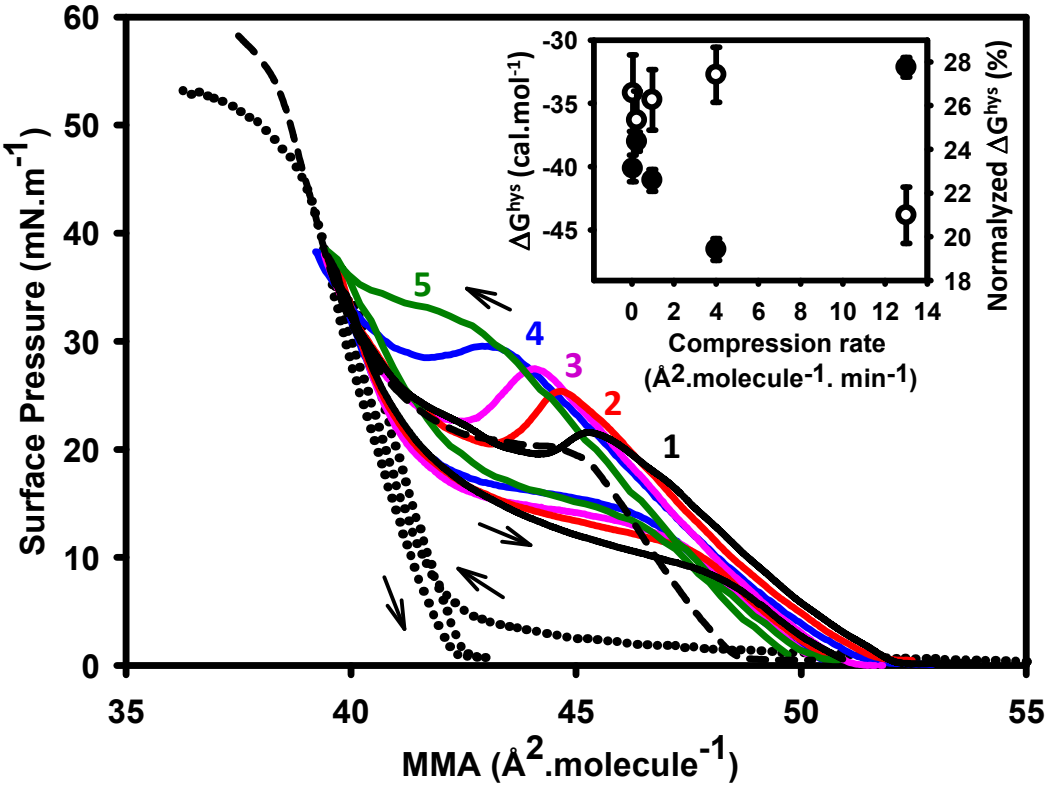

Figure 2. Hysteresis and kinetically restricted processes of *cis*-pCer monolayers. Compression/expansion cycles of *cis*-pCer at different compression rates are shown for *cis*-pCer films compressed and expanded at 0.05 (1, black), 0.2 (2, red), 1 (3,pink), 4 (4,blue) and 13 (5, green) Å^2.molecule^{-1}.min^{-1} and *trans*-pCer (black dotted line) compressed at 1 Å^2.molecule^{-1}.min^{-1}. The equilibrium compression isotherm of *cis*-pCer monolayers shown in figure 1 is reproduced here for comparison (black dashed line). The arrows indicate the time direction of the process, either compression or expansion. The plots show representative experiments that do not differ in more than 0.2 Å^2.molecule^{-1} from their replicas. The free energy related to the hysteresis process at different compression rates, expressed as cal.mol^{-1} (closed symbols) or as a percentage of the

compression free energy (open symbols), are plotted in the inset. The error bars correspond to SEM.

Further studies on the kinetic restriction observed for the S2 phase formation by *cis*-pCer were performed by compressing/expanding the film at different rates. When the film is compressed at a relatively fast rate, a pseudo-plateau occurs above 30 $mN.m^{-1}$ that appears as a regular phase transition (Figure 2, green line). However, in the expansion isotherm the transition plateau occurs under 20 $mN.m^{-1}$. When the compression/expansion rate is lowered to ≤ 4 $Å^2.molecule^{-1}.min^{-1}$ the compression curve does not show a plateau but a valley that is not observed in the expansion curves. This reflects the existence of kinetic limitations for the formation of the more condensed state S2 from S1; however, the reverse transition under expansion from the state S2 does not show kinetic restrictions.

Note that the lowering of the compression rate also induces a reduction of the depth of the valley, approaching closely the equilibrium compression curve (see Figure 2). This suggests that a compression rate slow enough to result in an equilibrium curve must exist, although the latter could not be experimentally accessed with our current set-up. The lowering of the compression rates also induces a lowering of the transition pressure, the latter also approaching that of the equilibrium isotherm.

The observations described strongly suggest a kinetically restricted transition from S1 (low surface pressure state) to S2 (high surface pressure state). The formation of S2 appears to be faster than the destabilization of S1: since molecules organized in state S2 occupy a smaller area than in S1, the transition occurring in the 4 - 0.05 $Å^2.molecule^{-1}.min^{-1}$ rate range leads to an apparent lowering of the surface pressure (valley). This would be a consequence of a depletion of molecules in the S1 state (continuous phase at the lower surface pressure end of the coexistence region) by generation of vacancy areas. These solid, hardly deformable states appear to respond slowly to molecular rearrangements required

to replenish the vacancies thus leading to the observed transient decrease of surface pressure under film compression.

According to NMR data by[34], *cis*-pCer show the capacity of forming an hydrogen-bonding network between the OH groups of C1 and C3 and bound water molecules. Then, the S1 $\rightarrow$ S2 phase transition may imply a dehydration of the *cis*-pCer polar region concomitant to braking of the H-bonding network. This dehydration process may involves a slow kinetics, giving account for the slow destabilization of the S1 *cis*-pCer phase.

This phenomenon is also reflected by the compressibility modulus of the *cis*-pCer compression isotherms at different compression rates. Figure 1b shows a notable drop of Cs^{-1} down to negative values. Our observations of compression isotherms constitute macroscopic approaches to molecular changes, even if mesoscopic lipid domains should occur during phase transitions. Then, the global rheological properties observed through the Cs^{-1} parameter may correspond to the continuous phase (S1 state under depletion), the discontinuous lipid domains (S2 growing domains) being invisible to such parameters until percolation or electrostatic repulsions take place.[42]

Conversely, during the expansion process, destabilization of state S2 appears to be faster than the rate of formation of S1, probably due to a slow hydration of the polar region of *cis*-pCer and formation of hydrogen bonding. Thus, no valley appears in the transition region of the expansion isotherms at any of the accessible rates studied (Figure 2). However, the S2-to-S1 transition occurs at a surface pressure below the transition pressure of the equilibrium isotherm; this further suggests that S2 is in a relatively long-lived state before the formation of S1 can be brought about by the considerable driving force of surface pressure steady lowering under expansion.

As seen in Figure 2, the path followed under compression of *cis*-pCer monolayers is different from the one observed during the expansion process, resulting in a marked hysteresis. Hysteresis occurs when the energy supplied to the monolayer upon film compression (ΔG_{comp}) is not equal to the energy returned by the system

during the expansion process (ΔG_{expan}). Thus, a certain amount of energy (ΔG^{hys}) becomes stored by the state adopted under compression as a part of the intermolecular interactions, and it is not returned under expansion. Such phenomena have been reported for protein or lipid-protein[38,43] and lipid–nanoparticle films and for synthetic amphiphilic molecules able to establish intermolecular hydrogen bonds.[44–46] For *cis*-pCer the excess free energy necessary for the film compression and S1-to-S2 phase transition may contain also the energy for dehydration and braking of the hydrogen bonding between the C1 and C2 hydroxyl group and water. This may be not fully reverted in the inverse process producing energetic hysteresis. Notably, no comparable effects were detected for *trans*-pCer, which cannot form such hydrogen-bonding network and for which hysteresis was very small (Figure 2).

The free energy stored by the system during compression decreases when the compression rate is progressively lowered from 4 to 0.05 $Å^2$.molecule^{-1}.min^{-1}, showing the progressive tendency to reversibility that should be expected for an equilibrium process. The ΔG^{hys} kept by the system under compression represents a relatively constant percentage of ΔG_{comp} (see inset in Figure 2), supporting the hypothesis of a dehydration process during the S1 $\rightarrow$ S2 phase transition involving a constant energy requirement. However, at the faster compression rate explored, ΔG^{hys} shows a lower value, representing only 20% of ΔG_{comp}, instead of ~ 26-28% observed for the slower compression rates. At such relatively fast compression-expansion rate the thermodynamic regime no longer follows a monotonic variation with the increase of the perturbation rate. This may reflect that the solid state formed at the fastest compression rates does not have the same properties of the S2 state originated at relatively lower compression rates.

Microscopy inspection of cis-pCer monolayers

Microscopy analysis at the mesoscopic level has become a major tool for analyzing the structure of lipid surfaces. However films containing large areas of solid or condensed phases are difficult to study by fluorescence microscopy since most

fluorescent probes contain bulky fluorophore moieties that are usually excluded from highly packed lipid states (S, LC or even liquid-ordered). Furthermore, the fluorescent probe may change the phase equilibrium, in particular when it is excluded from at least one of the coexisting phases.[47]

Brewster angle microscopy (BAM) however allows the exploration of Langmuir film heterogeneities in the absence of any probe through the analysis of film reflectivity [39,40]. BAM inspection of *trans*-pCer films shows, over a large range of surface pressures, a continuous, solid-like surface whose "optical" thickness increased from 1.73 to 1.80 (± 0.03) nm with the LC → S phase transition.[26] This change shows a close correlation with the reported tilted → untilted gel phase for bulk pCer dispersion by X-ray diffraction.[17]

In the present work, *cis*-pCer monolayers exhibit a clear S → S phase transition with characteristic microscopy features under BAM observation. Figure 3a-d shows pictures of *cis*-pCer monolayers along the compression under equilibrium conditions (allowing film relaxation for 30 min after each 5 $mN.m^{-1}$ increase). BAM images show lipid domains with different brightness. The effect is more evident at low surface pressures (S1 phase). Note that this effect was not observed for *trans*-pCer monolayers (Figure 3e).

For an isotropic medium at the interface plane, the reflected light has the same polarization plane as the incident light beam. This is not the case when the organization of the film is optically anisotropic and the symmetry axes of its molecular components are not in the normal to the interface (as observed for several chiral amphiphile films [46,48]). This generates a birefringence effect where the refractive indexes have different values in the direction of the hydrocarbon chains and in the orthogonal direction.[40] *Cis*-pCer monolayers show this birefringence phenomenon (Figure 3a-d and 4) strongly suggesting that the molecular axes are oriented in a different manner from the normal to the interface in the different domains of the S1 phase.

To test this hypothesis, we evaluated the brightness level of neighbouring domains at different orientations of the A-polariser. The films interact with the normally

polarized light, altering the resultant polarization plane, so that the reflected light becomes a function of the angle formed by the A-polariser and the normal plane (see Figure 3a-d, +45 and -45 °C). BAM images exhibit changes in the brightness of neighbouring domains of *cis*-pCer films observed with different orientations of the A-polariser, supporting the occurrence of highly ordered lipid domains oriented in different directions.

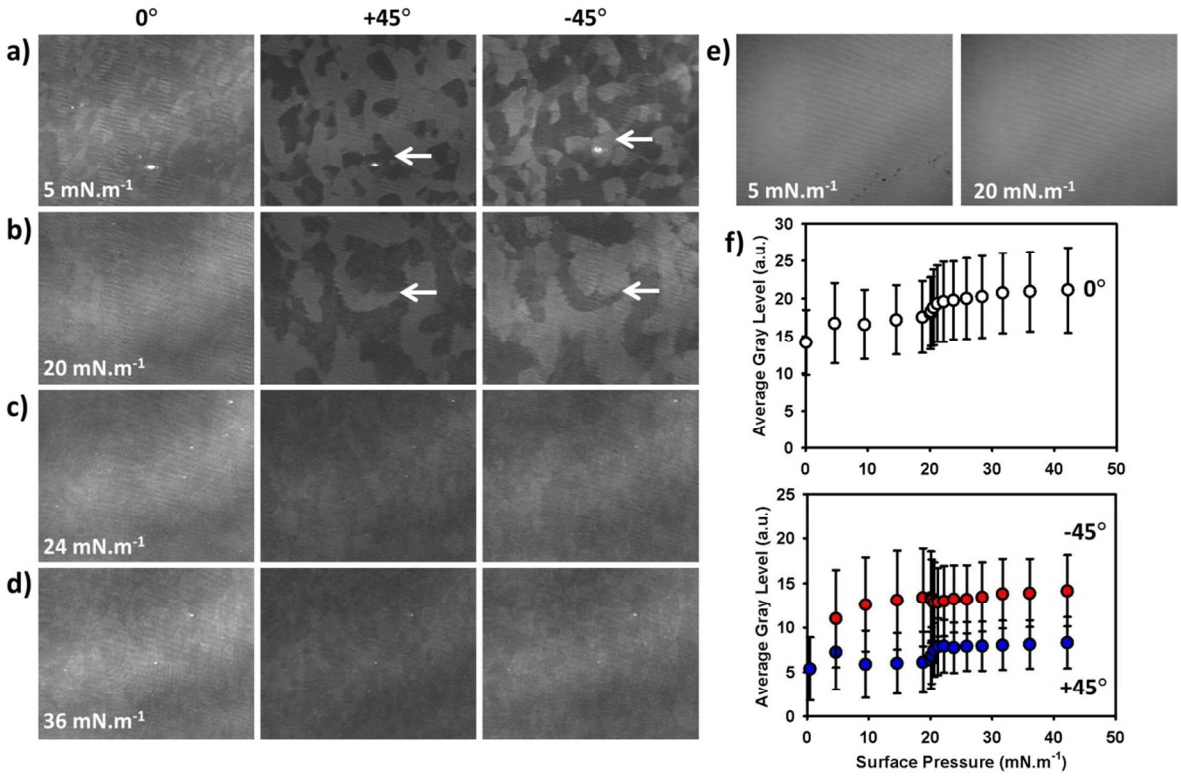

Figure 3. BAM images of *cis*-pCer monolayers at different surface pressures, observed through the A-polariser set to 0, +45° or -45°, as indicated. Arrows highlight the same lipid domain observed at different polariser set-ups. a-d) Representative images were taken from two independent experiments in which a 30 min relaxation at a constant MMA was allowed after reaching each target surface pressure as indicated (corresponding to points a-d in Figure 1c). e) For comparison *trans*-pCer monolayer images are shown at the surface pressure indicated and acquired through the A-polariser set to 0. Image size: 200 x 250 µm. For better visualization, the lower 0-70 grey level range (from the 0-255 original scale) was selected. f) Average grey level after background subtraction of *cis*-pCer BAM images along the compression process setting the A-polariser to 0 (open), +45° (blue circles) or -45° (red circles) from the plane normal. Data taken from two independent sets of experiments. Average values ± S.D.

A detailed analysis of the average grey level of each picture evidences a clear increase over the phase transition range together with a decrease in the differences of gray level between the A-polariser settings +45 and -45° (Figure 3f). This effect correlated with a decrease in the error bars of the +45 and -45° gray values, indicating a more upright position of the molecules with a lower azimuth in the S2 phase state, at surface pressures above the phase transition.

Altogether, our experimental data are consistent with the occurrence of a phase transition between a tilted crystalline-like structured phase occupying a relatively large molecular area (S1) and a less tilted solid state (S2) where *cis*-pCer molecules pack in a similar manner than its related isomer *trans*-pCer. The transition between two highly packed, but differently structured solid films having different kinetics of formation underlie the kinetically-limited features of *cis*-pCer monolayers.

Visualization of *cis*-pCer monolayers compressed under non-equilibrium conditions further highlights some of the differences observed in the above isothermal compression experiments. When *cis*-pCer films compressed at intermediate rates (within the range studied in figure 2) are explored by BAM the images show smaller area patches with different grey levels than under equilibrium conditions (compare Figure 3 and 4). This evidences that both S1 and S2 phase are formed with a less structured, or more amorphous, character, resembling what would be expected for 3D solids formed under a high-rate temperature drop. [49]

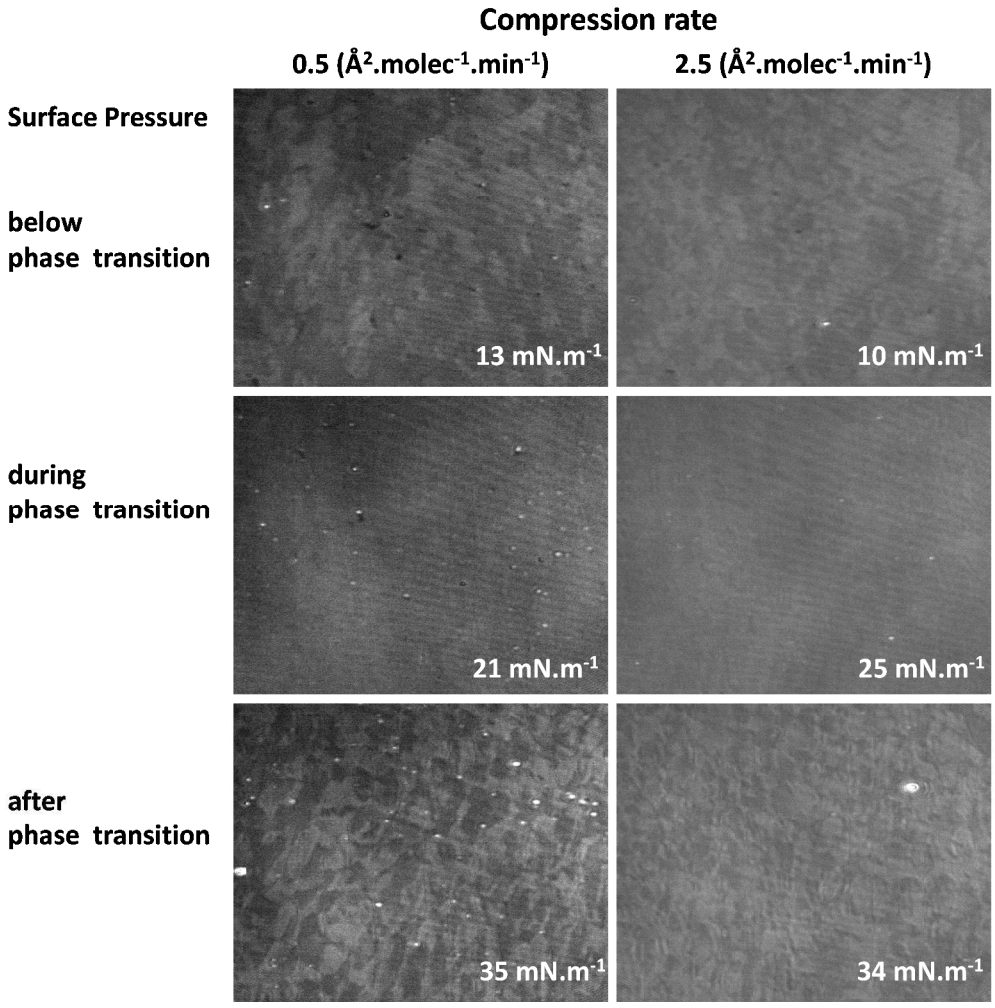

Figure 4. BAM images of *cis*-pCer monolayers compressed at different rates. Representative images were taken from two independent experiments at the indicated surface pressures. For a better visualization, the lower 0-70 grey level range (from the 0-255 original scale) was selected. Image size: 200 x 250 µm.

To get deeper insights into the nature of the less structured monolayers, further microscopy inspection was performed using atomic force microscopy (AFM). For this purpose, lipid monolayers were transferred onto a solid support after reaching the target surface pressure. Figure 5 shows a near-homogeneous film for both *cis*-pCer and *trans*-pCer at low surface pressure (5 mN/m). Some irregularly-shaped depressions in the film are observed, which are also present at higher surface pressures. Domain heterogeneity as seen in BAM images (figure 3a) is not

detected by AFM. This may be due to these domains keeping a constant thickness, or having thicknesses that differ in less than ≈0.2 nm, thus being undetectable to the AFM. The breaks in the Cer films were not observed by BAM, perhaps because they are produced during film transfer, unless they are too small to be detected by BAM

The evolution of the film by AFM under compression shows a notable change of the surface texture over the phase transition pressure range. Figure 5a shows that, in monolayers transferred at 20 mN/m, needle-like crystalline structures grow from a main axis at defined angles. The average height of the needles is 363±67 pm (see supplementary Figure 1). These crystalline structures appear less evident at higher surface pressures but are still visible at 30 mN/m. This finding supports the hypothesis of the pressure-induced growth of a solid phase (S2) within a primary, less structured, solid state (S1), in the surface pressure range where the transition is evident by isothermal compression and BAM. The crystalline needles may represent the initial nuclei from which the S2 phase grows during the compression process. Those thin structures observed by AFM were not observed by BAM, which has a 5-fold poorer resolution limit in the x-y coordinate. However, analysis of BAM images shows a subtle increase in the average reflectivity of the film during the S $\rightarrow$ S phase transition (see Figure 3e), which may account for the $\sim$ 0.3 nm thicker S2 needles in comparison with the S1 phase by AFM. Notably, this effect is not observed in *trans*-pCer monolayers, where a nearly-homogeneous phase is observed.

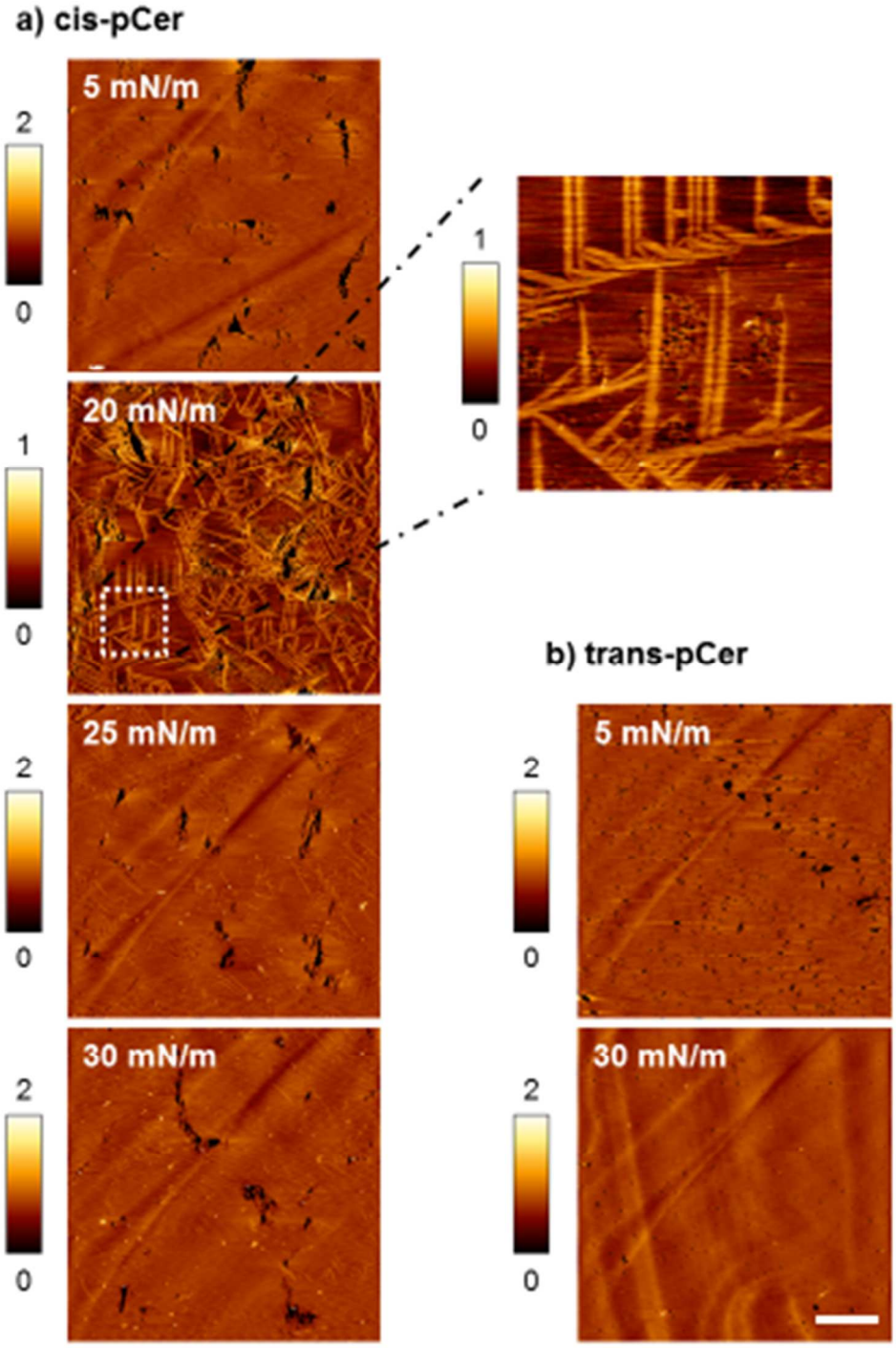

Figure 5. AFM visualization of *cis*-pCer monolayers transferred to solid support. Contact-mode height AFM images of c*is*-pCer (a) and *trans*-pCer (b) Langmuir films transferred to solid support at different surface pressures, as indicated. The films were compressed at 0.5 $Å^2$ $molec^{-1}$ min^{-1} and left to equilibrate for 30 min at constant lateral pressure prior to transfer. The images are representative samples of at least 4 independent experiments. Scale bar: 10 μm. Color bar in nm. Zoomed area = 10x10 μm.

Computational study of cis- and trans-pCer monolayers.

Atomistic molecular dynamics simulations of *cis*- and *trans*-pCer provide interesting insights into the behaviour of these lipids in monolayers at the air-water interface. Representative configurations of both kinds of molecules are shown in Figure 6, centre and right-hand columns. The distributions of the distances between the ends of the lipid tails and of the difference between the oxygen positions in C1-OH and C3-OH along the coordinate perpendicular to the monolayer are shown in the Supplementary Figure 2. Two important differences are observed. One is the more spread conformation of the *cis* over the *trans* molecule in the disordered state (see bottom left panel of Supplementary Figure 2). This explains the observation in Figure 1, that the MMA of *trans*-pCer can be considerably reduced (from ≈50 to ≈45 $Å^2$.$molecule^{-1}$) with a minimal increase in surface pressure, as compared with the changes observed with *cis*-pCer. The second interesting observation is that, for the *trans* isomer, only the hydroxyl group in C1 is in contact with the water, while both hydroxyls, in C1 and in C3, are accessible to the aqueous phase in the *cis* isomer. This confirms the NMR data by[34] according to which cis double bond twists the orientation of C1- with respect to C3-OH, thus weakening the hydrogen-bonding network formed between the two OH groups of *cis*-Cer and bound water molecules. This could in turn be related to some macroscopic properties of the *cis*-pCer, e.g. a weaker hydrogen-bonding network could facilitate the coexistence of different phases in the monolayer. A related important observation derived from the molecular dynamics simulations is provided by the whole system representations (Figure 6, left-hand side column). The *trans*-pCer monolayer (top) appears highly homogeneous, with a large proportion of the molecules organized in parallel arrays. In contrast the *cis*-pCer monolayer (bottom) shows coexisting ordered and disordered domains that could reflect the heterogeneous appearance of these samples under BAM observations (Figure 3).

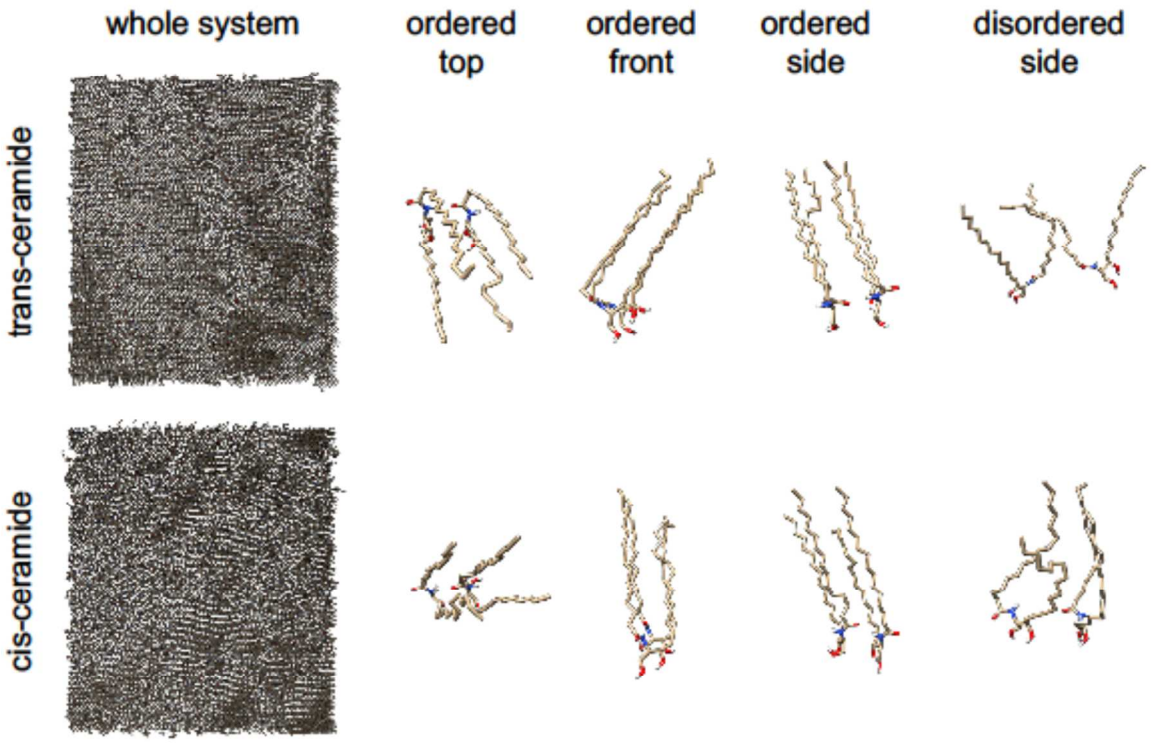

Figure 6. Representative configurations of lipids and the whole system for trans- and cis-ceramide monolayers at the air/water interface from computer simulations. (top; left) The whole system viewed from the lipid-tail side of the trans-pCer monolayer (air side of the air/water interface) with the lipids shown in gray. (top; center) A pair of representative lipid configurations from the ordered region (viewed from the top: lipid-tail side on top; the side and front: water/air interface on the bottom); and (top; right) a pair of neighboring lipid configurations representative of the disordered region of the monolayer. (bottom) The same for the cis-ceramide monolayers. The coordinates of the lipids for trans- and cis-ceramide monolayers are included in the Supporting Information files transtot50.pdb and cistot50.pdb, respectively.

Conclusions

Cis-pCer organized as a monomolecular film at room temperature shows clearly the occurrence of a particular S → S phase transition. A comparable phenomenon is not detected in *trans*-pCer. At low surface pressures, a crystalline-like tilted phase that occupies ~ 46 $Å^2$.$molecule^{-1}$ and with a surface rheology corresponding to a soft solid phase (S1), undergoes a kinetically restricted phase transition to a relatively long-lived tightly packed solid film (S2) with a molecular packing and rheology properties similar to the solid phase formed by *trans*-pCer. The slow destabilization of the S1 phase as well as the energetic hysteresis of the process may occur as a consequence of a slow dehydration and breaking of the hydrogen bonding network between the OH group of the C1 and C3 of *cis*-pCer and water molecules.[34] This transition occurs with the growth of needle-like crystals, which denotes a preferential orientation for the propagation of growth of the solid domains. Such solid phases resemble the phases described for *trans*-pCer in monolayers[26] and bulk suspensions,[17] which also show the presence of a metastable and a stable gel phase.

Both factors, the tilted azimuthal orientation of the *cis*-pCer in the film and its asymmetrical crystal growth reveal asymmetric intermolecular interactions which may originate in an optimal orientation for the formation of H-bonds between the sphingosine moieties of Cer. A weaker hability of *cis*-pCer to form intermolecular H-bonding and a more disordered organization in comparison with *trans*-pCer monolayers, as revealed by computational simulations, support the macroscopic S1 → S2 transition of *cis*-pCer monolayers. This kind of phenomena may be present in the solid phases formed by other sphingosine-based lipids such as *trans*-Cer, cerebrosides or sphingomyelin, perhaps in a way that has so far been scarcely accessible to experimental exploration since the solid phases formed might be rather similar in molecular area and thermodynamic parameters.

Acknowledgements

This work was supported in part by Consejo Nacional de Investigaciones Científicas y Técnicas (CONICET), Agencia Nacional de Promoción Científica y Tecnológica (ANPCyT, FONCyT PICT 2014-1627), and Secretary of Science and Technology of Universidad Nacional de Córdoba (SECyT-UNC) in Argentina (MLF and BM), and by the Spanish Ministry of Economy grants No. BFU 2015–66306-P (FMG and AA), CTQ 2017-85378-R (JLA and GF), and FIS 2015-68722-R (JMGV), and the Basque Government grants IT838-13, IT849-13.

Supporting information

Two supplementary figures complementing figures 5 and 6, and two pdb files containing the coordinates of the lipids in the monolayers shown in figure 6.

References

(1) Maggio, B.; Fanani, M. L.; Rosetti, C. M.; Wilke, N. Biophysics of sphingolipids II. Glycosphingolipids: an assortment of multiple structural information transducers at the membrane surface. *Biochimica et Biophysica Acta - Biomembranes*. 2006, pp 1922–1944.

(2) Maggio, B.; Borioli, G. a.; Del Boca, M.; De Tullio, L.; Fanani, M. L.; Oliveira, R. G.; Rosetti, C. M.; Wilke, N. Composition-driven surface domain structuring mediated by sphingolipids and membrane-active proteins. Above the nano- but under the micro-scale: mesoscopic biochemical/structural cross-talk in biomembranes. *Cell Biochem. Biophys.* **2008**, *50* (2), 79.

(3) Kolesnick, R. N.; Goñi, F. M.; Alonso, A. Compartmentalization of ceramide signaling: physical foundations and biological effects. *J. Cell. Physiol.* **2000**, *184*, 285.

(4) Venkataraman, K.; Futerman, A. H. Ceramide as a second messenger: sticky solutions to sticky problems. *Trends Cell Biol.* **2000**, *10* (10), 408.

(5) Grassmé, H.; Riethmüller, J.; Gulbins, E. Biological aspects of ceramide-enriched membrane domains. *Prog. Lipid Res.* **2007**, *46* (3–4), 161.

(6) López-Montero, I.; Monroy, F.; Vélez, M.; Devaux, P. F. Ceramide: from lateral segregation to mechanical stress. *Biochim. Biophys. Acta - Biomembr.* **2010**, *1798* (7), 1348.

(7) Goñi, F. M.; Alonso, A. Biophysics of sphingolipids I. Membrane properties of sphingosine, ceramides and other simple sphingolipids. *Biochim. Biophys. Acta - Biomembr.* **2006**, *1758* (12), 1902.

(8) Goñi, F. M.; Alonso, A. Effects of ceramide and other simple sphingolipids on membrane lateral structure. *Biochim. Biophys. Acta - Biomembr.* **2009**, *1788* (1), 169.

(9) Castro, B. M.; Prieto, M.; Silva, L. C. Ceramide: a simple sphingolipid with unique biophysical properties. *Prog. Lipid Res.* **2014**, *54* (1), 53.

(10) Fanani, M. L.; Hartel, S.; Maggio, B.; De Tullio, L.; Jara, J.; Olmos, F.; Oliveira, R. G. The action of sphingomyelinase in lipid monolayers as revealed by microscopic image analysis. *Biochim. Biophys. Acta - Biomembr.* **2010**, *1798* (7), 1309.

(11) Ale, E. C.; Maggio, B.; Fanani, M. L. Ordered-disordered domain coexistence in ternary lipid monolayers activates sphingomyelinase by clearing ceramide from the active phase. *Biochim. Biophys. Acta - Biomembr.* **2012**, *1818* (11), 2767.

(12) Silva, L. C.; Futerman, A. H.; Prieto, M. Lipid raft composition modulates sphingomyelinase activity and ceramide-induced membrane physical alterations. ***Biophys. J.*** 2009**, *96* (8), 3210.**

(13) Zhang, Y.; Li, X.; Becker, K. A.; Gulbins, E. Ceramide-enriched membrane domains--structure and function. *Biochim. Biophys. Acta - Biomembr.* **2009**, *1788* (1), 178.

(14) Härtel, S.; Fanani, M. L.; Maggio, B. Shape transitions and lattice structuring of ceramide-enriched domains generated by sphingomyelinase in lipid monolayers. *Biophys. J.* **2005**, *88* (1), 287.

(15) Fanani, M. L.; Härtel, S.; Oliveira, R. G.; Maggio, B. Bidirectional control of sphingomyelinase activity and surface topography in lipid monolayers. *Biophys. J.* **2002**, *83* (6), 3416.

(16) De Tullio, L.; Maggio, B.; Fanani, M. L. Sphingomyelinase acts by an area-activated mechanism on the liquid-expanded phase of sphingomyelin monolayers. *J. Lipid Res.* **2008**, *49* (11), 2347.

(17) Shah, J.; Atienza, J. M.; Duclos, R. I.; Rawlings, a V; Dong, Z.; Shipley, G. G. Structural and thermotropic properties of synthetic C16:0 (palmitoyl) ceramide: effect of hydration. *J. Lipid Res.* **1995**, *36* (9), 1936.

(18) Fidelio, G. D.; Maggio, B.; Cumar, F. A. Molecular parameters and physical state of neutral glycosphingolipids and gangliosides in monolayers at different temperatures. *Biochim. Biophys. Acta* **1986**, *854* (2), 231.

(19) Brown, R. E.; Brockman, H. L. Using monomolecular films to characterize lipid lateral interactions. *Methods Mol. Biol.* **2007**, *398*, 41.

(20) Wilke, N. Lipid monolayers at the air-water interface. In *Advances in Planar Lipid Bilayers and Liposomes*; Iglič, A., Kulkarni, C. V., Eds.; Academic

Press: Burlington, **2014**; *20*, pp 51–81.

(21) López-Montero, I.; Catapano, E. R.; Espinosa, G.; Arriaga, L. R.; Langevin, D.; Monroy, F. Shear and compression rheology of Langmuir monolayers of natural ceramides: solid character and plasticity. *Langmuir* **2013**, *29* (22), 6634.

(22) Catapano, E. R.; Arriaga, L. R.; Espinosa, G.; Monroy, F.; Langevin, D.; López-Montero, I. Solid character of membrane ceramides: a surface rheology study of their mixtures with sphingomyelin. *Biophys. J.* **2011**, *101* (11), 2721.

(23) Espinosa, G.; López-Montero, I.; Monroy, F.; Langevin, D. Shear rheology of lipid monolayers and insights on membrane fluidity. *Proc. Natl. Acad. Sci. U. S. A.* **2011**, *108* (15), 6008.

(24) Busto, J. V.; Fanani, M. L.; De Tullio, L.; Sot, J.; Maggio, B.; Goñi, F. M.; Alonso, A. Coexistence of immiscible mixtures of palmitoylsphingomyelin and palmitoylceramide in monolayers and bilayers. *Biophys. J.* **2009**, *97* (10), 2717.

(25) Dupuy, F.; Fanani, M. L.; Maggio, B. Ceramide N-acyl chain length: a determinant of bidimensional transitions, condensed domain morphology, and interfacial thickness. *Langmuir* **2011**, *27* (7), 3783.

(26) Fanani, M. L.; Maggio, B. Phase state and surface topography of palmitoyl-ceramide monolayers. *Chem. Phys. Lipids* **2010**, *163* (6), 594.

(27) Peñalva, D. A.; Oresti, G. M.; Dupuy, F.; Antollini, S. S.; Maggio, B.; Aveldaño, M. I.; Fanani, M. L. Atypical surface behavior of ceramides with nonhydroxy and 2-hydroxy very long-chain (C28-C32) PUFAs. *Biochim. Biophys. Acta - Biomembr.* **2014**, *1838* (3), 731.

(28) Brockman, H. L.; Momsen, M. M.; Brown, R. E.; He, L.; Chun, J.; Byun, H.-S.; Bittman, R. The 4,5-double bond of ceramide regulates its dipole potential, elastic properties, and packing behavior. *Biophys. J.* **2004**, *87* (3), 1722.

(29) Sot, J.; Goñi, F. M.; Alonso, A. Molecular associations and surface-active properties of short- and long-N-acyl chain ceramides. *Biochim. Biophys. Acta - Biomembr.* **2005**, *1711* (1), 12.

(30) Chen, H. C.; Mendelsohn, R.; Rerek, M. E.; Moore, D. J. Fourier transform infrared spectroscopy and differential scanning calorimetry studies of fatty acid homogeneous ceramide 2. *Biochim. Biophys. Acta - Biomembr.* **2000**, *1468* (1–2), 293.

(31) Školová, B.; Januìššová, B.; Zbytovská, J.; Gooris, G.; Bouwstra, J.; Slepička, P.; Berka, P.; Roh, J.; Palát, K.; Hrabálek, A.; Vávrová, K. Ceramides in the skin lipid membranes: length matters. *Langmuir* **2013**, *29* (50), 15624.

(32) Alonso, A.; Goñi, F. M. The Physical Properties of Ceramides in Membranes. *Annu. Rev. Biophys.* **2018**, *47* (1), 633..

(33) El Bawab, S.; Bielawska, A.; Hannun, Y. A. Purification and characterization of a membrane-bound nonlysosomal ceramidase from rat brain. *J. Biol. Chem.* **1999**, *274* (39), 27948.

(34) Phillips, S. C.; Triola, G.; Fabrias, G.; Goñi, F. M.; DuPré, D. B.; Yappert, M. C. cis- versus trans-ceramides: effects of the double bond on conformation and H-bonding interactions. *J. Phys. Chem. B* **2009**, *113* (46), 15249.

(35) Bianco, I. D.; Fidelio, G. D.; Maggio, B. Modulation of phospholipase A2 activity by neutral and anionic glycosphingolipids in monolayers. *Biochem. J.* **1989**, *258* (1), 95.

(36) Gaines, G. L. *Insoluble Monolayers at Liquid-Gas interfaces*; Prigogine, I., Ed.; Interscience Publishers: NY, 1968.

(37) Peñalva, D. A.; Wilke, N.; Maggio, B.; Aveldaño, M. I.; Fanani, M. L. Surface behavior of sphingomyelins with very long chain polyunsaturated fatty acids and effects of their conversion to ceramides. *Langmuir* **2014**, *30* (15), 4385.

(38) Grasso, E. J.; Oliveira, R. G.; Maggio, B. Rheological properties of regular insulin and aspart insulin Langmuir monolayers at the air/water interface: condensing effect of Zn2+ in the subphase. *Colloids Surfaces B Biointerfaces* **2014**, *115*, 219.

(39) Lheveder, C.; Meunier, J.; Henon, S. In *Physical Chemistry of Biological Interfaces*; Baszkin, A., Norde, W., Eds.; Marcel Dekker, Inc.: New York, Basel, 2000.

(40) Vollhardt, D. Phases and phase transition in insoluble and adsorbed monolayers of amide amphiphiles: Specific characteristics of the condensed phases. *Curr. Opin. Colloid Interface Sci.* **2014**, *19* (3), 183.

(41) Hoopes, M. I.; Noro, M. G.; Longo, M. L.; Faller, R. Bilayer structure and lipid dynamics in a model stratum corneum with oleic acid. *J. Phys. Chem. B* **2011**, *115* (12), 3164.

(42) Caruso, B.; Mangiarotti, A.; Wilke, N. Stiffness of lipid monolayers with phase coexistence. *Langmuir* **2013**, *29* (34), 10807.

(43) Borioli, G. A.; Maggio, B. Surface thermodynamics reveals selective structural information storage capacity of c-Fos-phospholipid interactions. *Langmuir* **2006**, *22* (4), 1775.

(44) Vico, R. V.; Fernando Silva, O.; De Rossi, R. H.; Maggio, B. Molecular organization, structural orientation, and surface topography of monoacylated beta-cyclodextrins in monolayers at the air-aqueous interface. *Langmuir* **2008**, *24* (15), 7867.

(45) Vico, R. V.; De Rossio, R. H.; Maggio, B. PM-IRRAS assessment of the compression-mediated orientation of the nanocavity of a monoacylated beta-cyclodextrin in monolayers at the air-water interface. *Langmuir* **2010**, *26* (11), 8407.

(46) Mottola, M.; Vico, R. V.; Villanueva, M. E.; Fanani, M. L. Alkyl esters of L-ascorbic acid: Stability, surface behaviour and interaction with phospholipid

monolayers. *J. Colloid Interface Sci.* **2015**, *457*, 232.

(47) Cruz, A.; Vázquez, L.; Vélez, M.; Pérez-Gil, J. Influence of a fluorescent probe on the nanostructure of phospholipid membranes: dipalmitoylphosphatidylcholine interfacial monolayers. *Langmuir* **2005**, *21* (12), 5349.

(48) Vollhardt, D.; Fainerman, V. B. Characterisation of phase transition in adsorbed monolayers at the air/water interface. *Adv. Colloid Interface Sci.* **2010**, *154* (1–2), 1.

(49) Flemings, M. C.; Shiohara, Y. Solidification of undercooled metals. *Mater. Sci. Eng.* **1984**, *65* (1), 157.

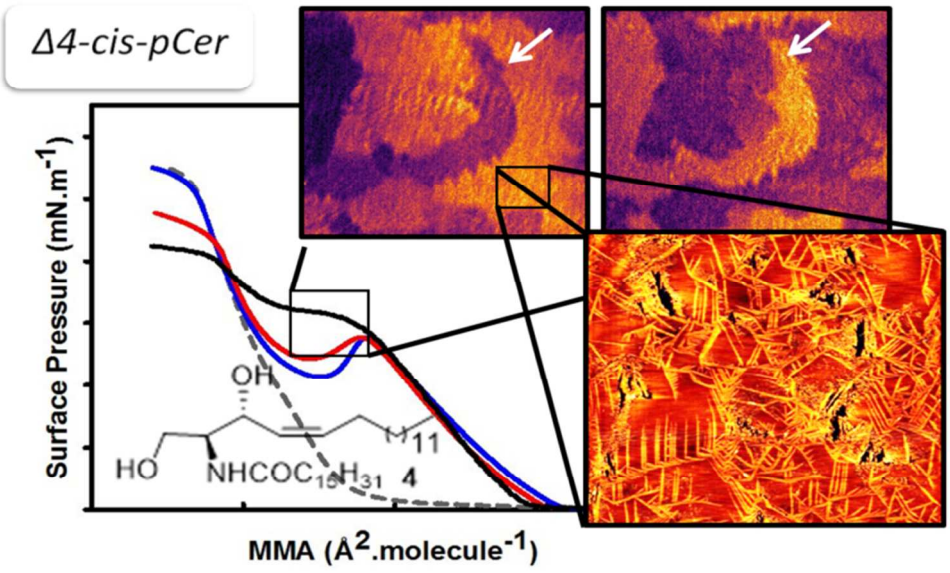

76x44mm (300 x 300 DPI)